EUROPHYSICS LETTERS 1 April 2004

Europhys. Lett., **66** (1), pp. 48–54 (2004)
DOI: 10.1209/epl/i2003-10185-0

Beam fanning used to study thermal disorder and decay of polar structures in the ferroelectric relaxor $Sr_{0.61}Ba_{0.39}Nb_2O_6$

M. Goulkov[1], O. Shinkarenko[1], T. Granzow[2], Th. Woike[2] and M. Imlau[3]

[1] *Institute of Physics - Science Ave. 46, 03650 Kiev-39, Ukraine*
[2] *Institute for Mineralogy, University of Cologne - Cologne, Germany*
[3] *Department of Physics, University Osnabrück - Osnabrück, Germany*

(received 25 April 2003; accepted in final form 8 January 2004)

PACS. 42.65.Hw – Phase conjugation; photorefractive and Kerr effects.
PACS. 77.80.-e – Ferroelectricity and antiferroelectricity.
PACS. 78.20.Jq – Electrooptical effects.

Abstract. – A new photorefractive approach using the temperature evolution of beam fanning to study the polar structure of the ferroelectric relaxor strontium-barium-niobate (SBN) undergoing the ferroelectric-paraelectric phase transition is proposed. A strong temperature dispersion of the decay of polar structures of different sizes is observed. We compare our results with those obtained by other measurement methods to show their dependence on the size distribution of the polar structures.

The connection between the optical properties and the polar structure of electro-optic crystals is at the very heart of many physical effects, starting from almost trivial birefringence to the most difficult photorefractive phenomena. It is therefore not surprising that the growing demand for efficient optical materials for applications such as holographic data storage or frequency conversion has led to increased research activities in this field. The most prominent example are certainly attempts to use ferroelectric crystals such as lithium niobate with a pre-determined polar structure, so-called periodically poled crystals, to produce the desired optical effects [1]. However, although much effort has been spent to produce specific polar configurations that might be favorable for applications, the opposite direction, the examination of a given polar structure by electro-optic methods, has been a bit neglected. Still, it was demonstrated that such methods are very effective to investigate changes in the polar structure of ferroelectrics both on a macroscopic and on a microscopic scale, especially for ferroelectric-paraelectric phase transitions [2].

The ferroelectric relaxor $Sr_{0.61}Ba_{0.39}Nb_2O_6$ (SBN) is interesting from both points of view: It displays strong electro-optic properties that make it a good candidate for applications, and it exhibits a phase transition from a ferroelectric to a paraelectric phase at comparably low temperatures, facilitating an easy examination of phase transition properties. Due to its relaxor nature, its polar structure does not vanish abruptly when the crystal is heated above the phase transition. Instead, it possesses an intermediate "relaxor" regime in a wide temperature

interval extending from the ferroelectric to the paraelectric phase, where the macroscopic polarization of the crystal gradually relaxes to zero [3,4]. An experimental determination of the phase transition temperature is a particular problem for the relaxor SBN: Different measurement methods give different values, which generally are referred to as T_M. For example, in SBN doped with 0.66 mol% cerium, T_M detected from the maximum of the dielectric permittivity ε at 100 Hz (ε-method) equals $T_M = 67\,^\circ$C [5]. Determination of T_M from the inflection point of the spontaneous electric polarization P_3 (P-method) [6] gives $T_M \approx 57\,^\circ$C. The smallest value, $T_M = 52\,^\circ$C, has been received by the photorefractive method (PR-mehtod) [7], where T_M is detected from the intensity maximum of the light-induced scattering distribution. We assume that the dispersion of T_M measured by various methods has two major reasons: i) different spatial scales in the polar structure display different thermal-decay behavior when SBN undergoes the phase transition, and ii) different methods used to determine the phase transition temperature are sensitive to different polar scales.

The thermal decay of the polar structure in relaxor SBN is quite diffusive. First, in the vicinity of the phase transition the increasing thermal energy overcomes the cooperative interaction between ferroelectric domains. Then, at higher temperatures, long-range interactions between elementary electric dipoles fail, and ferroelectric domains are replaced by so-called polar clusters. These clusters at first retain the orientation of the original domain configuration. As a result, SBN exhibits a macroscopic electric polarization even above the phase transition. The spatial disorder and further erosion of clusters with increasing temperature results in a decay of the polar structure and vanishing electric polarization. Note that clusters, defining the polar structure in the relaxor regime, give rise to a rich variety of ferroelectric domains in the crystal bulk when it is cooled to the ferroelectric phase. The existence of bulk domains in SBN has been experimentally proven [8]. Poling in high external electric fields causes an ordering of the domains in one direction, allowing for a nonzero electric polarization P_3 along the crystallographic $\boldsymbol{c}$-axis. The size Λ of the domains in the ferroelectric phase and of polar clusters in the relaxor regime varies from several nm to several μm [9, 10]. Polar structures of different sizes should decay differently with temperature. This will necessarily result in a considerable smearing of the integrated response of the crystal when detecting T_M by different methods. Since different methods differ in their sensitivity on polar structures of different particular sizes, a strong dispersion of T_M obtained from various methods is observed. For a better understanding of the decay processes of the polar structure, it is therefore desirable to develop a method which will separately measure the thermal evolution of polar structures with different sizes. Below, we propose a new effective method to analyze the disorder/decay of these polar structures in SBN on scales ranging from 0.4 μm to 50 μm based on measurements of temperature changes of light-induced scattering (or "beam fanning" [11]) and show that a decay of different polar scales takes place in a temperature interval $45\,^\circ\text{C} \le T \le 60\,^\circ$C.

Beam fanning is a kind of light-induced wide-angle scattering emerging in some ferroelectric crystals pumped by a single laser beam. In $Sr_{0.61}Ba_{0.39}Nb_2O_6$ (SBN), efficient beam fanning appears from an extraordinarily polarized beam propagating normally to the polar $\boldsymbol{c}$-axis of the crystal and forms a spatially asymmetric polarization-isotropic light strip oriented opposite to the $\boldsymbol{c}$-axis. The conventional model [12] explains beam fanning as a result of the direct coupling of coherent optical noise (or primary scattering) with the transmitted part of the pump beam on noisy refractive index gratings recorded due to the photorefractive effect [13]: Light interference patterns formed by pump and primary scattering waves induce free electrons in the crystal bulk, diffusion of nonuniformly photoexcited carriers forms space-charge fields E_{diff}, the fields modulate the index of refraction via the linear electro-optic coefficient r_{33}: $\Delta n = -\frac{1}{2} n_e^3 r_{33} E_{\text{diff}}$. The electro-optic properties of SBN strongly depend on the electric

polarization P_3, since r_{33} can be written as

$$r_{33} = 2g_{33}P_3\varepsilon_{33}\varepsilon_{\mathrm{o}}\,, \tag{1}$$

where g_{33} is the quadratic electro-optic coefficient. According to eq. (1), photorefractive recording remains possible only if $P_3 \neq 0$. Therefore, the relaxor regime in SBN allows the existence of a photorefractive effect and, respectively, of beam fanning above the phase transition.

The diffusion mechanism of photorefraction causes a $\pi/2$-shift between refractive index gratings and initial light patterns. Thus, an effective two-wave coupling with unidirectional energy transfer between waves interacting on such gratings occurs. In SBN, the pump-scattering coupling results in an amplification of primary scattering with a negative projection of the propagation vector on the $\boldsymbol{c}$-axis at the expense of the pump beam, and in the depletion of scattering with a positive projection in favor of the pump beam. The first part of the scattered light is described by negative scattering angles measured from the normal to the crystal, the second part is described by positive scattering angles. The intensity of two scattering waves symmetrically propagating out of the crystal at the scattering angles $\pm\theta_{\mathrm{s}}$ equals

$$I_{\mathrm{s}}^{\pm\theta_{\mathrm{s}}} = I_{\mathrm{so}}^{\pm\theta_{\mathrm{s}}} \exp\big[\mp\Gamma(\theta_{\mathrm{s}})l\big], \tag{2}$$

where l is the interaction length and Γ the coupling coefficient describing the energy exchange between the two waves. The signs "$-$" or "$+$" indicate that scattering is either depleted or amplified. The exact equations for Γ for beam fanning in SBN can be found in [14]. The pre-exponential factor $I_{\mathrm{so}}^{\pm\theta_{\mathrm{s}}}$ in eq. (2) is the intensity of primary scattering seeding beam fanning in the $\pm\theta_{\mathrm{s}}$-direction.

Primary scattering is a result of diffraction/refraction of the incident beam on optical inhomogeneities of the crystal [12]. According to the model of primary scattering developed for SBN [15], the scattering mostly originates on local anomalies $\delta n = -\frac{1}{2}n_{\mathrm{e}}^3 r_{33}E_{\mathrm{int}}$ of the refractive index n_{e} induced by internal fields E_{int} via the electro-optic effect. Since the fields E_{int} are also responsible for the formation of ferroelectric domains [16,17], local changes of n_{e} are mostly located at domain tips. Domains in SBN are oriented only along the $\boldsymbol{c}$-axis, and the polar structure of the crystal can be considered as a large number of sequences of domains of equal size distributed more or less regularly in this direction. Consequently, scattering sources built into such polar structures also form a large number of spatially periodical (or quasiperiodical) δn-sequences along the polar axis. The periods Λ of a particular δn-sequence equals the characteristic dimension of domains in the sequence. Note that results of studies of Rayleigh scattering in SBN also indicate that the scattering originates in the bulk of the crystal, and scattering centers are arranged in rows parallel to the $\boldsymbol{c}$-axis [18]. Diffraction on such periodical structures aligned in rows results in primary scattering propagating at the scattering angles $\theta_{\mathrm{s}} = 2\arcsin(\lambda/(2\cdot\Lambda))$. The spatial arrangement of polar structures in SBN also affects the electric polarization P_3 and thereby the amplitude of local refractive index anomalies δn via the linear electro-optic coefficient r_{33} (see eq. (1)). The bulk nature of primary scattering and the direct correlation of changes in the polar structure and primary scattering has been confirmed by a detailed study of beam fanning in SBN at different temperatures and external electric fields [15,19]. It has been shown that perfectly aligned domain- and δn-sequences result in stronger primary scattering, while primary scattering from irregular δn-sequences on disordered polar structures is less effective. The importance of the decay of the polar structure increases near the phase transition, where the disorder of ferroelectric domains results in drastic changes of primary scattering. Therefore, the intensity I_{so} is a suitable parameter to study the temperature evolution of polar structures in SBN passing the phase transition.

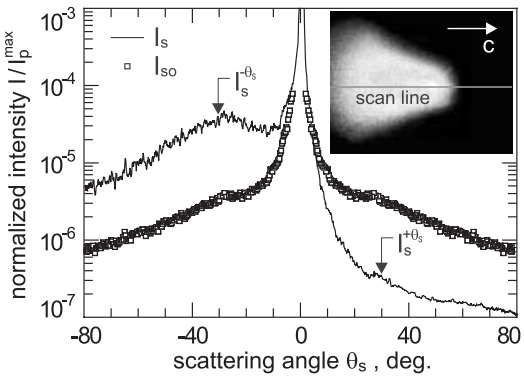

Fig. 1

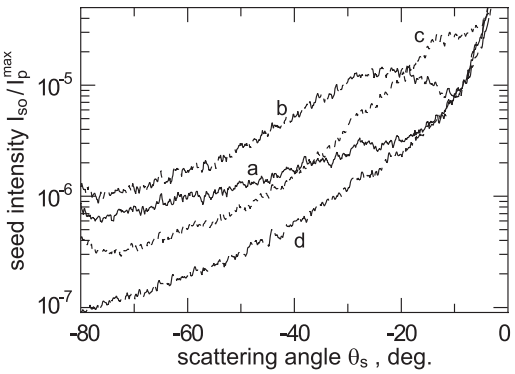

Fig. 2

Fig. 1 – Angular distribution of beam fanning intensity I_s and seed scattering intensity I_{so} at $T = 52\,^\circ$C. Inset: Picture of total scattering distribution with scan line.

Fig. 2 – Angular distribution of primary scattering $I_{so}(\theta_s)$ for $T = 15\,^\circ$C (a), $45\,^\circ$C (b), $56\,^\circ$C (c) and $68\,^\circ$C (d).

To receive I_{so} from a beam fanning experiment, one has to take into account that the alignment of scattering centers along the polar axis determines a symmetric distribution of the primary scattering in the $\pm c$-direction: $I_{so}^{-\theta_s} = I_{so}^{+\theta_s} = I_{so}^{\theta_s}$. Thus, the square-root product of $I_s^{-\theta_s}$ and $I_s^{+\theta_s}$ will give the primary scattering intensity $I_{so}^{\theta_s}$ equal for both waves:

$$I_{so}^{\theta_s} = \sqrt{I_s^{+\theta_s} I_s^{-\theta_s}}\,. \tag{3}$$

With this equation, the angular distribution of the primary scattering at the temperature T can be extracted from the corresponding angular distribution of the beam fanning intensity.

Measurements were performed with a single crystal of SBN doped with 0.66 mol% cerium with dimensions of 5.65 mm × 0.7 mm × 2.75 mm $\parallel \boldsymbol{c}$. The unexpanded beam of a He-Ne laser ($\lambda = 633$ nm, $I_p = 70\,\mathrm{mW/cm^2}$, diameter $d = 1.5$ mm) impinged normally on the $\boldsymbol{c}$-axis, having extraordinary polarization in the crystal. A typical beam fanning pattern observed on a screen behind the crystal is shown in the inset of fig. 1. The angular distribution of the scattering intensity was measured by a photodetector rotated around the sample at a distance of $L = 5.5$ cm: The plane of movement is shown in the inset by the scan line. The sample temperature was varied with a thermoelectric element in the range of $10\,^\circ\mathrm{C} \le T \le 150\,^\circ$C with an absolute accuracy of $0.3\,^\circ$C.

The solid line in fig. 1 shows the beam fanning profile at $T = 52\,^\circ$C. The scattering intensity possesses a maximum at negative angles θ_s and extremely small values at positive θ_s. The peak at $\theta_s = 0^\circ$ corresponds to the transmitted pump beam. The squares show the corresponding profile of the primary scattering I_{so} extracted from the I_s-curve with eq. (3). I_{so} is symmetric in θ_s, but exhibits a strong angular dependence, indicating that structures of different scale contribute differently to the total intensity of primary scattering: δn-sequences at small domains (large θ_s) result in weaker primary scattering than δn-sequences associated with large domains (small θ_s). This result is quite apparent, since larger domains are associated with larger local fields E_{int} and larger amplitudes δn.

The temperature evolution of I_{so} is illustrated in fig. 2, where curves a-d are I_{so}-profiles shown for $\theta_s < 0$ for $T = 15\,^\circ$C, $45\,^\circ$C, $56\,^\circ$C and $68\,^\circ$C, respectively. We define the total

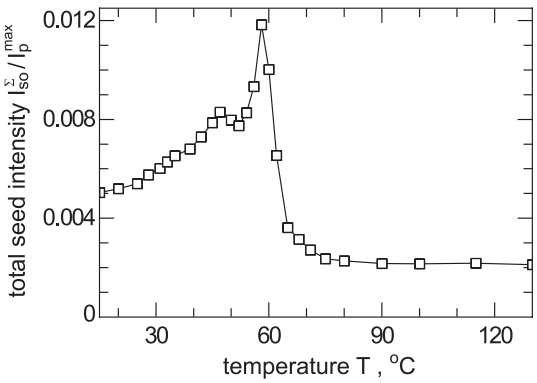

Fig. 3

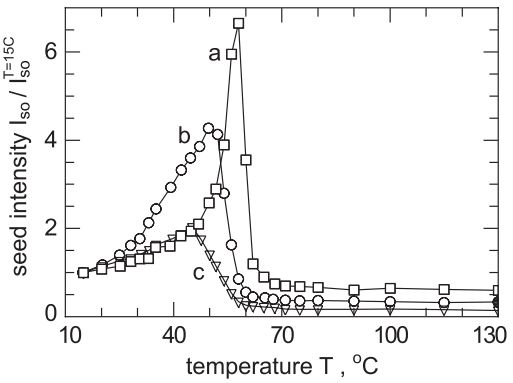

Fig. 4

Fig. 3 – Temperature dependence of the total intensity of primary scattering $I_{\rm so}^{\Sigma}(\theta_{\rm s})$.

Fig. 4 – $I_{\rm so}^{\theta_s}(T)$ of the seed scattering propagating at $\theta_{\rm s} = 10°$ (a), $30°$ (b) and $60°$ (c).

primary scattering intensity $I_{\rm so}^{\Sigma}$ as the integral over a single $I_{\rm so}$-profile (exempting the central peak from the pump beam) at a particular temperature T. It describes the averaged state of the polar structure in the crystal. The dependence of $I_{\rm so}^{\Sigma}$ on T is shown in fig. 3. At the same time, $I_{\rm so}^{\theta_{\rm s}}$ describes the efficiency of the diffraction of the pump beam on δn-sequences with the spatial period Λ. It is therefore another measure of the actual state of polar scales (domains/clusters) of the particular size $\Lambda = \lambda/(2\,\sin(\theta_{\rm s}/2))$. The temperature dependencies of $I_{\rm so}$ at $\theta_{\rm s} = 10°$, $30°$ and $60°$ are shown in fig. 4. For better comparison, all curves are normalized at $T = 15\,°$C. The initial ascending part of all three curves is due to an increase of r_{33} with temperature [20, 21]. It results in growing amplitudes of local δn-anomalies, causing an enhancement of primary scattering. The maximum of each curve can be interpreted as the temperature where the spatial disorder of the corresponding polar structure begins. Photorefractive properties of the crystal start to diminish, and light-induced scattering is suppressed. The error in measuring $T(I_{\rm so}^{\rm max})$ does not exceed $2\,°$C over the entire temperature interval. The descending parts of the curves point to the further decay of polar structures stimulated by the increased thermal energy of the crystal. As follows from fig. 4, small-scale structures (larger $\theta_{\rm s}$)

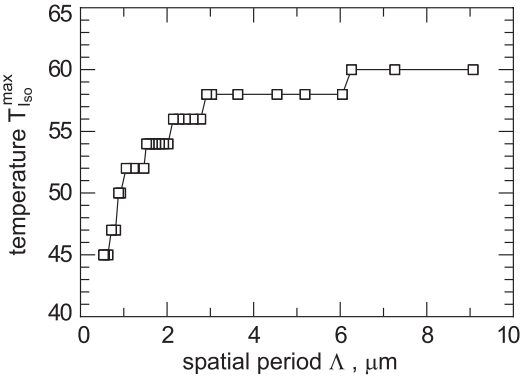

Fig. 5 – Temperature of the maximum of $I_{\rm so}^{\theta_s}(T)$ *vs.* spatial period Λ.

exhibit spatial disorder and vanish at lower temperatures than large-scale structures (smaller θ_s). Figure 5 shows the correspondence between the spatial period Λ and the temperature T_M at which the intensity $I_{so}^{\theta_s}$ crosses its maximum. The curve is restricted to $4^\circ \leq \theta_s \leq 80^\circ$ to avoid both the influence of the transmitted pump beam at small angles and of internal reflections at the inner crystal faces at large angles. According to fig. 5, spatial disorder of the smallest polar structures occurs at $T_M = 45\,^\circ$C, while the spatial orientation of the largest structures remains stable up to $T_M = 60\,^\circ$C. Such big dispersion of the thermal decay of polar structures over Λ (fig. 5) unambiguously illustrates the relaxor behavior of SBN, and at the same time is a key point for understanding the dispersion of T_M determined in SBN from different methods.

Due to the different approaches in measuring the phase transition temperature, the ε-, P- and PR-methods mentioned in the introductory part respond differently to changes on different scales Λ of the polar structure. A comparison of fig. 3 and fig. 5 with T_M values measured from these three methods allows to evaluate their Λ-sensitivity. The first maximum of $I_{so}^{\Sigma}(T)$ is located at $T = 48\,^\circ$C, indicating that the sensitivity of the total primary scattering to changes in the polar structure is limited to scales $\Lambda \geq 0.85\,\mu$m: The contribution of structures with smaller Λ seems to be too small to considerably affect I_{so}^{Σ}. The nearest value of $T_M = 52\,^\circ$C was measured with the PR-method, exploiting the strong dependence of the total intensity and the spatial distribution of the scattered light on the value of P_3 and therefore on changes in the polar structure of the crystal. According to fig. 5, the PR-method responds to a spatial disorder in polar structures with $\Lambda \geq 1\,\mu$m, which can also be considered as the spatial limit for this method. The second and largest maximum of $I_{so}^{\Sigma}(T)$ is at $T = 58\,^\circ$C, close to $T_M = 57\,^\circ$C measured by the pyroelectric P-method. Thus, one can conclude that this method is sensitive to spatial changes in the range $\Lambda \geq 2.85\,\mu$m. The highest value, $T_M = 67\,^\circ$C, is detected by the ε-method from measurements of the dielectric permittivity. In fig. 3, this temperature corresponds to the deep tail in the $I_{so}^{\Sigma}(T)$-dependence, and at the same time does not fit any data in fig. 5. The ε-method at frequencies of 100 Hz is the least sensitive and measures noticeable changes only when the polar structure is almost shattered, because the largest contribution to the dielectric response is always received from a totally fragmented polar structure with a very high concentration of cluster walls in the crystal volume.

In conclusion, detailed information on changes in the polar structure of SBN:Ce during the ferroelectric-paraelectric phase transition is received from the study of the temperature evolution of beam fanning. The disorder/decay of polar structures of different scales occurs in a wide temperature interval from 45 °C to 60 °C. This is the reason for the variations in the characteristic temperatures T_M measured by different methods. The photorefractive method thus offers a unique insight into the change of polar structures on a scale of $0.6\,\mu\text{m} < \Lambda < 9\,\mu$m during the phase transition.

* * *

This work is supported by the DFG (SPP1056, WO618/3-3) and INTAS (01-0173).

REFERENCES

[1] Odoulov S., Tarabrova T., Shumelyuk A., Naumova I. I. and Chaplina T. O., *Phys. Rev. Lett.*, **84** (2000) 3294.
[2] Lehnen P., Kleemann W., Woike T. and Pankrath R., *Eur. Phys. J. B*, **14** (2000) 633.
[3] Smolenskij G. A., Isupov V. A., Agranovskaya A. I. and Popov S. N., *Sov. Phys. Solid State*, **2** (1961) 2584.
[4] Kuroda S. and Kubota K., *J. Phys. Chem. Solids*, **42** (1980) 573.

[5] Dec J., Kleemann W., Woike Th. and Pankrath R., *Eur. Phys. J. B*, **14** (2000) 627.
[6] Granzow T., Dörfler U., Woike Th., Wöhlecke M., Pankrath R., Imlau M. and Kleemann W., *Appl. Phys. Lett.*, **80** (2002) 470.
[7] Goulkov M., Granzow T., Dörfler U., Woike Th., Pankrath R. and Imlau M., *J. Opt. Soc. Am. B*, **57** (2002) 14.
[8] Fogarty G., Steiner B., Cronin-Golomb M., Laor U., Garrett M. H., Martin J. and Uhrin R., *J. Opt. Soc. Am. B*, **13** (1996) 2636.
[9] Lehnen P., Kleemann W., Woike Th. and Pankrath R., *Phys. Rev. B*, **64** (2001) 224109.
[10] Lehnen P., Dec J., Kleemann W., Woike Th. and Pankrath R., *Ferroelectrics*, **268** (2002) 113.
[11] Feinberg J., *J. Opt. Soc. Am.*, **72** (1982) 46.
[12] Voronov V. V., Dorosh I. R., Kuz'minov Yu. S. and Tkachenko N. V., *Sov. J. Quantum Electron.*, **10** (1980) 1346.
[13] Kukhtarev N. V., Markov V. P., Odoulov S. G., Soskin M. S. and Vinetskii V. L., *Ferroelectrics*, **22** (1979) 961.
[14] Obuhovski V. V. and Stoyanov A. V., *Sov. J. Quantum Electron.*, **12** (1985) 563.
[15] Goulkov M., Granzow T., Dörfler U., Woike Th., Imlau M. and Pankrath R., *Appl. Phys. B*, **76** (2003) 407.
[16] Chynoweth A. G., *Phys. Rev.*, **117** (1969) 1235.
[17] Granzow T., Woike Th., Wöhlecke M., Imlau M. and Kleemann W., *Phys. Rev. Lett.*, **89** (2002) 127601.
[18] Prokert F. and Schlage R., *Phys. Status Solidi B*, **87** (1978) 179.
[19] Goulkov M., Imlau M., Granzow T. and Woike Th., *J. Appl. Phys.*, **94** (2003) 4763.
[20] Tomita Y., *Opt. Mater.*, **281** (1995) 4.
[21] Goulkov M., Granzow T., Dörfler U., Woike Th., Imlau M. and Pankrath R., *Opt. Commun.*, **218** (2003) 173.